X-ray-induced Scintillation Governed by Energy Transfer Process in Glasses

Masai, Hirokazu; Okada, Go; Torimoto, Aya; Usui, Takaaki; Kawaguchi, Noriaki; Yanagida, Takayuki

SCIENTIFIC REPORTS

OPEN

X-ray-induced Scintillation Governed by Energy Transfer Process in Glasses

Received: 4 September 2017
Accepted: 20 December 2017
Published online: 12 January 2018

Hirokazu Masai[1], Go Okada[2], Aya Torimoto[3], Takaaki Usui[3], Noriaki Kawaguchi[2] & Takayuki Yanagida[2]

The efficiency of X-ray-induced scintillation in glasses roughly depends on both the effective atomic number Z_{eff} and the photoluminescence quantum efficiency Q_{eff} of glass, which are useful tools for searching high-performance phosphors. Here, we demonstrate that the energy transfer from host to activators is also an important factor for attaining high scintillation efficiency in Ce-doped oxide glasses. The scintillation intensity of glasses with coexisting fractions of Ce^{3+} and Ce^{4+} species is found to be higher than that of a pure-Ce^{3+}-containing glass with a lower Z_{eff} value. Values of total attenuation of each sample indicate that there is a non-linear correlation between the scintillation intensity and the product of total attenuation and Q_{eff}. The obtained results illustrate the difficulty in understanding the luminescence induced by ionizing radiation, including the energy absorption and subsequent energy transfer. Our findings may provide a new approach for synthesizing novel scintillators by tailoring the local structure.

Phosphors are a kind of energy converters that generate light in a broad range of wavelengths from ultraviolet (UV) to infrared (IR). Although most phosphors possess the ability to convert light[1–35], some phosphors emit light as a result of mechanical stress[36,37]. Conventional phosphors are classified into two types: phosphors excited by UV or visible light[2–26] and phosphors excited by ionizing radiation[21–35]. For the latter, the photon energy is far beyond the band gap of materials and radiation-induced luminescence is brought about by energy transfer from the host matrix to activators[38–41]. Therefore, X-ray-induced scintillation is a complex process involving absorption of X-rays in the matrix and scintillation in the activators. The absorption of X-rays by a material, i.e. the total attenuation of ionizing radiation, which can be expressed in terms of an absorption cross-section, is proportional to the density of the material, ρ, and the fourth-power of effective atomic number of the material, Z_{eff}[4,38,39]. On the other hand, the scintillation efficiency, η, is typically expressed as $\eta = \beta_{e\text{-}h} \cdot S_{trans} \cdot Q_{eff}$, where $\beta_{e\text{-}h}$, S_{trans}, and Q_{eff} are the efficiencies of the processes for generating electron-hole pairs (generation of the secondary particles), transferring the energies of the secondary particles to luminescent centres, and exciting and emitting light at luminescent centres, respectively. The value of Q_{eff} is conventionally referred to as the internal quantum efficiency of photoluminescence (PL). Generally, the development of scintillators mainly focuses on the values of Z_{eff} and Q_{eff} because it is difficult to discuss quantitatively the efficiencies for the electron-hole generation or energy transfer processes. This is the reason why most studies have been performed using lanthanide-doped garnet crystals.

On the other hand, our group has focused on amorphous materials. Owing to their wide chemical composition range and good formability, glasses can be good candidates for detection of ionizing radiation[27–29]. One of the glasses reported for phosphor applications is a Ce-doped lithium borosilicate glass[27]. Although this type of glass contains no heavy element, it is a good reference for the following reasons: (1) Since the glass can be prepared in an inert atmosphere, clear emission properties of Ce^{3+} are observed. (2) The Q_{eff} values of the glasses are sufficiently high to discuss the changes of the scintillation efficiency. (3) Both B_2O_3 and SiO_2 can make glass networks, which correlates with the energy absorption and transfer process to the activators. (4) Valence states of Ce can be quantitatively discussed by using X-ray absorption near edge structure (XANES) analyses due to the lack of heavy cations whose absorption regions may overlap. A change in the compositional fraction of B_2O_3 and

[1]National Institute of Advanced Industrial Science and Technology, 1-8-31 Midorigaoka, Ikeda, Osaka, 563-8577, Japan. [2]Nara Institute of Science and Technology, 8916-5 Takayama-cho, Ikoma, Nara, 630-0192, Japan. [3]Institute for Chemical Research, Kyoto University, Gokasho, Uji, Kyoto, 611-0011, Japan. Correspondence and requests for materials should be addressed to H.M. (email: hirokazu.masai@aist.go.jp)

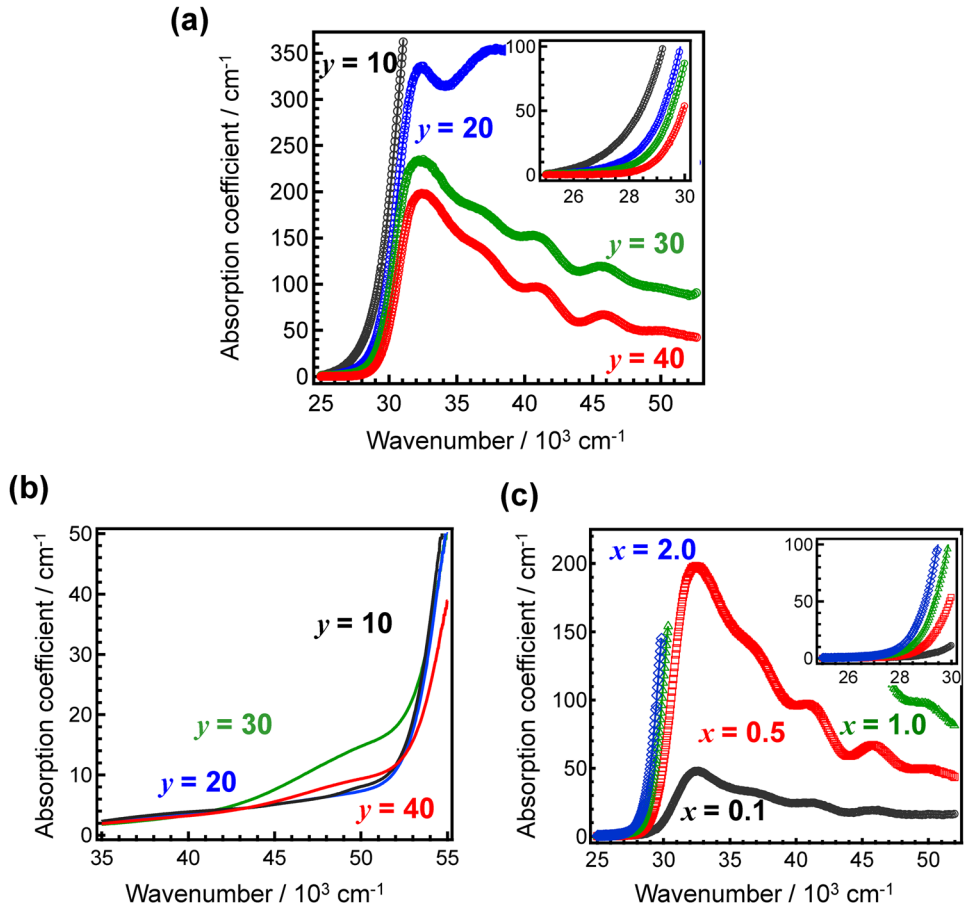

Figure 1. Optical absorption spectra of 0.5Ce:LBS*y* glasses. Optical absorption spectra of (**a**) 0.5Ce:LBS*y* glasses, (**b**) non-doped LBS*y* glasses and (**c**) *x*Ce:LBS40 glasses. The insets in Fig. 1(a) and (c) show zoomed-in view of the spectra at the optical absorption edge of these glasses.

SiO_2 is equivalent to a change in the value of Z_{eff}. Therefore, it is worthwhile to examine the PL and scintillation properties of Ce^{3+} in this glass system.

The aim of this study is to investigate the relationship between the valence state of activators in the lithium borosilicate glasses possessing different Z_{eff} values and the PL and scintillation efficiency. In order to discuss the valence state of cerium, the *Ce^{3+} ratio* in the glasses is introduced and defined as the ratio of the Ce^{3+}concentration to the sum of the concentrations for Ce^{3+} and Ce^{4+}. Based on several analytical data, we have found that there is an anomalous relationship between the scintillation properties and the chemical composition of glass.

Results

The chemical composition of the present glass system is xCe^{3+}-40Li_2O–$y$$B_2O_3$–(60-$y$)$SiO_2$ (in molar ratio), where an excess amount of Ce is added. Herein, the general glass system is abbreviated as *x*Ce:LBS*y*. First, we examined several Ce-doped Li_2O-B_2O_3-SiO_2 glasses in order to change the Z_{eff} value. An increase in the amount of SiO_2 increases the value of Z_{eff}, which determines the effective absorption of X-ray energy. The chemical composition and the nominal Z_{eff} values of these glasses are listed in Table S1. Figure 1(a) shows the optical absorption spectra of 0.5Ce:LBS*y* glasses at room temperature (RT) for different values of *y*. Comparison of the absorption spectra for 0.5Ce:LBS*y* glasses with those of non-doped LBS*y* glasses (Fig. 1(b)) demonstrates that most of the absorption is due to the addition of Ce. Furthermore, the shape of the spectra in Fig. 1(a) changes considerably with the value of *y* (i.e. the B_2O_3-SiO_2 ratio). On the other hand, Fig. 1(c) shows that the shape of the spectra slightly changes with the value of *x* (i.e. the Ce concentration)[27]. As shown in the inset of Fig. 1(c), when the chemical composition of LBS*y* is fixed, the optical absorption edge is slightly red-shifted with increasing amounts of Ce^{3+} due to be a broadening of the tail, i.e. a local coordination change (see Fig. S1). However, as shown in the inset of Fig. 1(a), the absorption coefficient at the tail region is largely red-shifted with increasing SiO_2 fractions. Therefore, it is expected that the absorption shape depends on both parameters *x* and *y*. Since the absorption tail of Ce^{4+} is observed at low energy regions[28,29], it is assumed that the red-shift of the absorption tail is correlated with the generation of Ce^{4+} species. Clear absorption bands are observed for LBS30 and LBS40 glasses. After a peak deconvolution using six absorption peaks with a half-width at half-maximum of approximately 2250 cm^{-1}, we found that the photon energy of each excitation peak is almost the same. The results suggest that the Ce^{3+} coordination is almost the same for both glasses and that the activators are dispersed homogenously in the glass matrix.

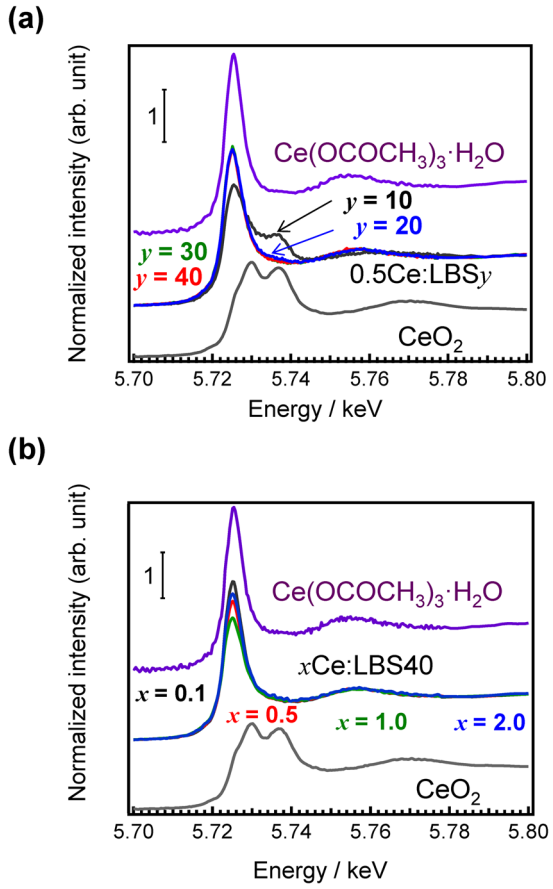

Figure 2. Ce XANES spectra of *x*Ce:LBS*y* glasses. Cerium L_{III}-edge XANES analysis of (**a**) 0.5Ce:LBS*y* glasses and (**b**) the *x*Ce:LBS40 glasses along with data for $Ce(OCOCH_3)_3{\cdot}H_2O$ and CeO_2.

In order to examine the valence state, we measured Ce L_{III}-edge XANES spectra of 0.5Ce:LBS*y* glasses, as shown in Fig. 2(a). These white lines change with the B_2O_3-SiO_2 ratio, especially near $y = 10$. The shape of the spectrum for the 0.5Ce:LBS40 glass is very similar to that of $Ce(OCOCH_3)_3{\cdot}H_2O$, as shown in Fig. S2, and noticeable differences for varying Ce concentrations are not observed (Fig. 2(b)). We can, therefore, conclude that the valence state of almost all (>95%) Ce centres in these LBS40 glasses are Ce^{3+} states, which is independent of the Ce concentration. Although precise fitting is difficult, the *Ce^{3+} ratio* of these glasses can be evaluated by spectra deconvolution using the spectra of $Ce(OCOCH_3)_3{\cdot}H_2O$ and CeO_2. Using these two reference materials, the *Ce^{3+} ratios* can be calculated as shown in Fig. 3. In the case of Ce:LBS30 and LBS40 glasses, the valence state of Ce is mostly the trivalent state. However, when the SiO_2 fraction increases, the *Ce^{3+} ratio* decreases. It is notable that the XANES spectrum of the 0.5Ce:LBS10 glass is very similar to that of the 0.5Ce:LBS40 glass prepared in air (Fig S3), and that the *Ce^{3+} ratio* is less than 40 %, although the preparation of 0.5Ce:LBS10 was performed in an Ar atmosphere.

Figure 4 shows PL and PL excitation (PLE) spectra of 0.5Ce:LBS*y* glasses at RT. The wavenumbers of both the excitation and emission peaks of Ce^{3+} for the present glass are lower than those in phosphate glasses[19,20] while higher than those in silicate glasses[20]. As the B_2O_3 fraction decreases, both peaks are slightly red-shifted, i.e. a smaller excitation energy induces a smaller emission energy. This might be correlated with the behaviour of the optical absorption spectra shown in Fig. 1(a), in which the absorption tail red-shifts with decreasing B_2O_3 fraction. Figure 5 shows contour plots of the PL-PLE spectra of 0.5Ce:LBS*y* glasses, where the PL intensity was normalized in order to understand the shapes of the spectra. The vertical and horizontal axes show the photon wavenumbers of excitation and emission, respectively. The fact that the excitation band is broad suggests that it is associated with the continuous excitation band, which is characteristic of Ce^{3+} states. However, as shown in Figs 4 and 5, the spectrum shape of the LBS10 glass is quite different from the shapes of the spectra for other B_2O_3 fractions. Irregularities associated with the LBS10 glass are also evident in the PL decay curves of *x*Ce:LBS*y* glasses shown in Fig. 6(a) for different B_2O_3 fractions. Specifically, a clear deviation from the linearity of the decay curves is observed for a B_2O_3 fraction of $y = 10$ shown in Fig. 6(b) and Fig S4. The decay constants of *x*Ce:LBS*y* glasses are summarized in Table S2. The internal quantum efficiencies Q_{eff} of *x*Ce:LBS*y* glasses are shown in Table S3 and Fig. 7. The values of Q_{eff} roughly depend on the Ce concentration and variations of Q_{eff} are probably due to differences in the local coordination state.

Figure 8(a) shows X-ray induced scintillation spectra of 0.5Ce:LBS*y* glasses obtained by and irradiation dose of 10 Gy. The scintillation intensities are normalized using the volume of the sample. We have confirmed that

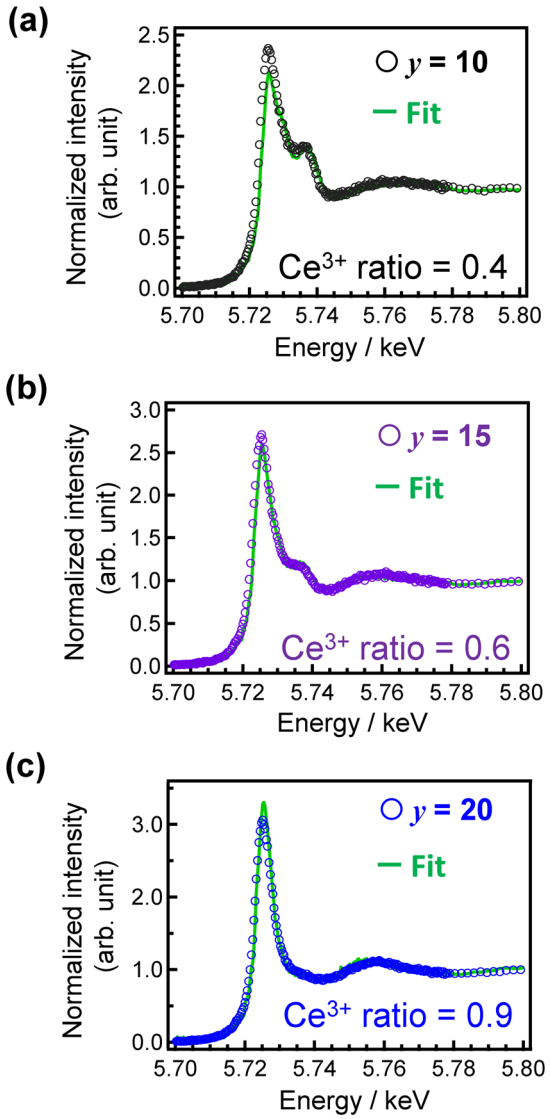

Figure 3. Cerium L_{III} XANES spectra of 0.5Ce:LBS*y* glasses along with fitting curves constructed by combination of XANES spectra of $Ce(OCOCH_3)_3{\cdot}H_2O$ and CeO_2.

the scintillation spectra were unchanged during irradiation and that there is a linear relationship between the irradiation dose and the scintillation intensity (Fig. S5(a) and (b)). Figure 8(a) also shows that emission peak wavenumbers of Ce^{3+} red-shift with decreasing B_2O_3 fraction, as was observed in the PL spectra. It is noteworthy that the emission peak area of the 0.5Ce:LBS10 glass is much larger than that of the 0.5Ce:LBS40 glass, although we have confirmed that many Ce species are oxidized into Ce^{4+} during melting. In order to discuss the Ce^{3+} *ratio* quantitatively, the values of Q_{eff}, and the scintillation peak area (normalized to the peak area of the 0.5Ce:LBS40 glass) are plotted in Fig. 8(b) as a function of Z_{eff} (bottom axis) and the B_2O_3 fraction (upper axis). It is evident that the scintillation intensity is proportional to Z_{eff} and inversely proportional to Q_{eff} and the Ce^{3+} *ratio*.

Discussion

We have found that the chemical composition of glass affects the valence state of the activator in glasses. The results clearly suggest that the average Ce^{3+} *ratio* is affected by the chemical composition of glass, i.e. the macroscopic basicity of glass. In order to explain the results, we use the concept of the 'optical basicity' defined by Duffy[42,43]. Optical basicity, i.e. the average basicity of oxides in the glass, is a concept based on the polarization of electrons. The idea of basicity of glasses is sometimes useful for evaluation of the physical properties of bulk glasses. The optical basicity of Li_2O, B_2O_3, and SiO_2 are reported to be 1, 0.42, and 0.48, respectively[43]. Therefore, when the optical basicity of glass increases by substitution of SiO_2 for B_2O_3, it is expected that an oxidation reaction of Ce^{3+} into Ce^{4+} occurs even in an Ar atmosphere. Since the starting materials of glass can affect the valence state of Ce cations[29], it is not possible to reach a direct conclusion from the observed phenomena. However, an increase of the optical absorption in SiO_2-rich glasses is expected to be brought about by a redox reaction transforming Ce^{3+} into Ce^{4+}.

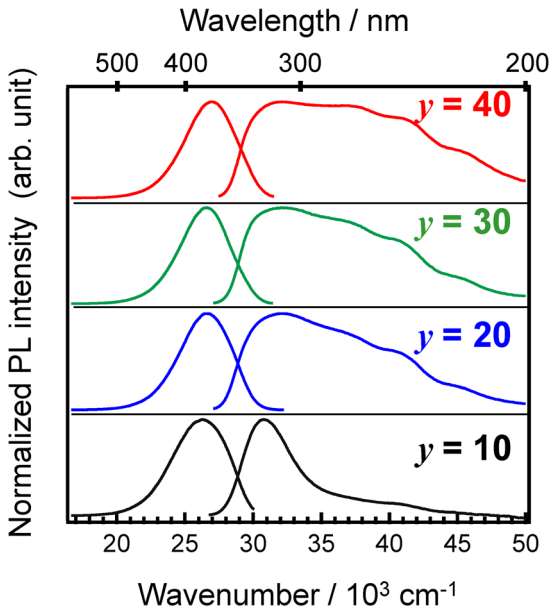

Figure 4. Photoluminescence-PLE spectra of 0.5Ce:LBS*y* glasses. The excitation and monitored wavenumbers correspond to the peaks of each spectrum.

To the best of our knowledge, the physics of ionizing radiation is still unclear because of the complexity of the process. Therefore, research on scintillators is often conducted by focusing on specific parameters. Although Q_{eff} is generally a useful parameter to develop scintillators, Z_{eff} has been found to play a more dominant role for X-ray-induced scintillators[34].

As mentioned above, an increase in the SiO_2 fraction causes an increase of Z_{eff}, which in turn increases the effective absorption of X-rays. Figure 9 shows the X-ray-induced scintillation peak area of *x*Ce:LBS*y* glasses as a function of the product $\rho \cdot Z_{eff}^4$. Since the dopant concentration is less than 2 mol%, the density of glass, ρ, shown in Table S4[44] can be used for the discussion. With the exception of Ce:LBS10 glasses, in which a decrease in scintillation intensity is observed due to the strong self-absorption in the visible region, the scintillation peak areas are roughly dependent on the Ce concentration. Although the value of Q_{eff} for the 0.5Ce:LBS10 glass is much lower than that of the 0.5Ce:LBS40 glass because of the generation of Ce^{4+} species, the scintillation peak area of the 0.5Ce:LBS10 glass is higher than the peak areas of most 0.5Ce:LBS*y* glasses in Fig. S9.

Figure 10(a) shows the total attenuation with coherent scattering of 0.5Ce:LBS*y* glasses, which was calculated using a previously published fomula[45] that takes into account the influence of Z_{eff}. The energy spectrum of the X-rays used in the present study[46–48] is also shown in the figure with a scale given on the right axis. Here, the X-ray source is a conventional X-ray tube with a W target and a Be window. In the energy region of irradiated X-rays, the total attenuation of the 0.5Ce:LBS10 glass is the highest among the present samples. Moreover, the attenuation values without coherent scattering exhibit a similar tendency. Here, we determined the total absorption energy using the following expression:

$$\zeta = \int EN_0(E)\frac{\mu_{EA}(E)}{\mu_T(E)}[1 - \exp\{\mu_T(E) \cdot t\}]dE \quad (1)$$

where ζ is the absorbed energy in the sample along the irradiation axis per unit area, $\boldsymbol{E}$ is the incident radiation energy, $\boldsymbol{N}_0$ is the number of incident photons per unit area, $\mu_T(\boldsymbol{E})$ is the total attenuation coefficient of the sample, μ_{EA} is the energy absorption coefficient of sample, and t is the thickness of the sample.

Figure 10(b) shows the total absorption energy, $\zeta_{relative}$, relative to that of the 0.5Ce:LBS10 glass. In the present X-ray energy region, the value of ζ for the 0.5Ce:LBS10 glass is approximately 1.2 times larger than that of the 0.5Ce:LBS40 glass. As mentioned above, the scintillation intensity I_{scinti} is a product of the total absorption energy ζ and the scintillation efficiency $\eta = \beta_{e\text{-}h} \cdot S_{trans} \cdot Q_{eff}$ and is given by

$$I_{scinti} = \zeta \cdot \beta_{e-h} \cdot S_{trans} \cdot Q_{eff} \quad (2)$$

Since we have no quantitative information about the values of $\beta_{e\text{-}h}$ and S_{trans}, their product, $(\beta_{e\text{-}h} \cdot S_{trans})$, is treated as a coefficient that can be evaluated using I_{scinti}, $\zeta_{relative}$, and Q_{eff}, and represents the efficiency for generating electron-hole pairs followed by energy transfer to luminescent centres in each glass. Using the values depicted in Figs 3(b) and 4(b), we have found that the value of $(\beta_{e\text{-}h} \cdot S_{trans})$ for the 0.5Ce:LBS10 glass is more than 14 times larger than that of the 0.5Ce:LBS40 glass (see right axis of Fig. 4(b)). In other words, the absorbed X-ray energy is not converted into scintillation photons effectively in 0.5Ce:LBS40 glasses.

Plausible reasons for the low conversion efficiency are the physical parameters of non-doped LBS glasses shown in Table S4[44]. Since the molar volume of the LBS10 glass is smaller than that of the LBS40 glass, the network

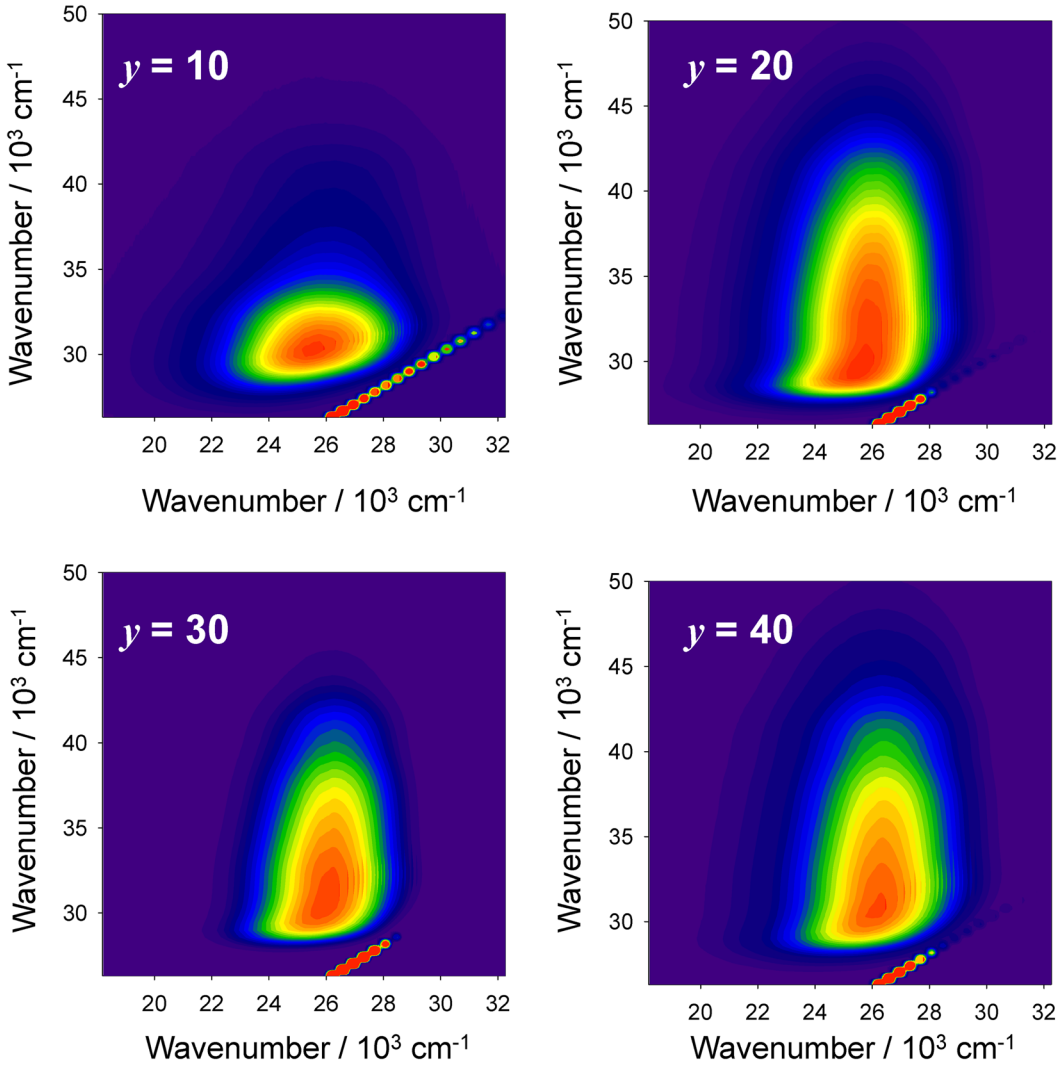

Figure 5. Contour plots of the PL-PLE spectra of 0.5Ce:LBS*y* glasses. The vertical and horizontal axes represent excitation and emission wavenumbers, respectively.

of the LBS10 glass is spatially denser than that of the LBS40 glass, i.e. there is larger free volume in the LBS40 glass. If there is no large difference in the phonon vibration energies of LBS*y* glasses, the free volume in the glasses may work as an attenuator and inhibit the effective energy transfer to activators. On the other hand, another reason for the low conversion efficiency is the storage mechanism of irradiated energy proposed by Yanagida[34]. It was reported that a B_2O_3-containing glass exhibits storage luminescence by X-ray irradiation[35]. Because the irradiated energy is converted into scintillation, storage luminescence, or thermal vibration (non-radiative relaxation), high storage luminescence means low scintillation. Considering that the origin of storage luminescence is defects in glasses, we speculate that there are many defects that affect the energy transfer process to activators in B_2O_3-rich glass. As shown in Fig. S6 and Table S5, there are only small differences in the band gaps for LBS*y* glasses and these differences cannot provide a plausible explanation for changes in the conversion efficiencies.

Recent studies have suggested that the fraction of Ce^{4+} in scintillators has an effect on scintillation properties[49–52] and several of them claimed that coexistence of Ce^{3+} and Ce^{4+} is important for high scintillation efficiency[49–51]. However, if the coexistence of Ce^{3+} and Ce^{4+} was a critical factor for determining the intensity, the correlation between chemical composition and scintillation intensity, as shown in Fig. 3(a), would be quite different; i.e. Ce:LBS*y* glasses would exhibit similar intensities with the exception of the Ce:LBS10 glass. Therefore, the present results do not support the hypothesis that coexistence of Ce^{3+} and Ce^{4+} is important for high scintillation efficiency, at least in the present glass system. In turn, this work shows that the energy transfer process of the generated charged secondary particles to activators is important for attaining high scintillation efficiency. Therefore, tailoring the energy transfer process is expected to enable fabrication of high-performance scintillators.

Conclusion

We have examined PL and X-ray-induced scintillation properties of several Ce-doped lithium borosilicate glasses. It was confirmed that only Ce^{3+} valence states exist in Ce:LBS40 glasses and that the Ce^{3+} *ratio* decreases with increasing SiO_2 fraction in the glasses. The oxidation reaction in the glass melt in an inert atmosphere can be

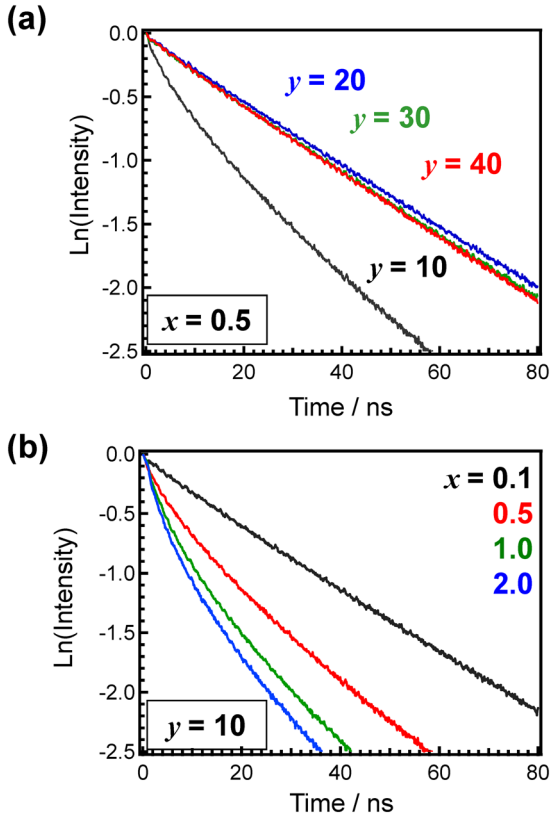

Figure 6. Photoluminescence decay curves of *x*Ce:LBS*y* glasses. Photoluminescence decay curves of (**a**) 0.5Ce:LBS*y* glasses and (**b**) *x*Ce:LBS10 glasses. The excitation and monitored wavenumbers (wavelengths) are 29,400 cm^{-1} (340 nm) and 25,000 cm^{-1} (400 nm), respectively.

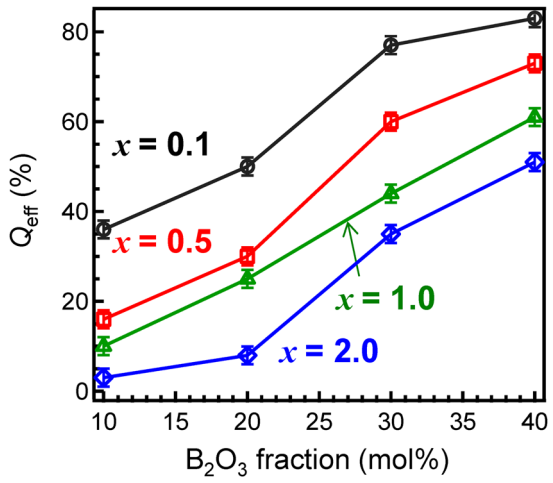

Figure 7. Quantum efficiency of *x*Ce:LBS*y* glasses as a function of the B_2O_3 fraction.

explained by the optical basicity of the glass, and the amount of Ce^{4+} generated is the origin of the absorption tail in the visible region of the absorption spectra. Although the value of Q_{eff} for the Ce:LBS10 glass is the smallest among all Q_{eff} values for the present LBS glasses, the scintillation intensity of the Ce:LBS10 glass is the highest because it has the highest attenuation values. In terms of the emission mechanism of scintillators, the effective energy conversion after absorbing the ionizing radiation is prevented in the B_2O_3-rich glasses. Such energy transfer path will be important for further materials design of radiation detectors.

Methods

Preparation of Ce-doped lithium borosilicate glass. The xCe^{3+}-$40Li_2O$–xB_2O_3–$(60-y)SiO_2$ (*x*Ce:LBS*y*) glasses were prepared according to a conventional melt-quenching method by employing a platinum crucible[24]. A

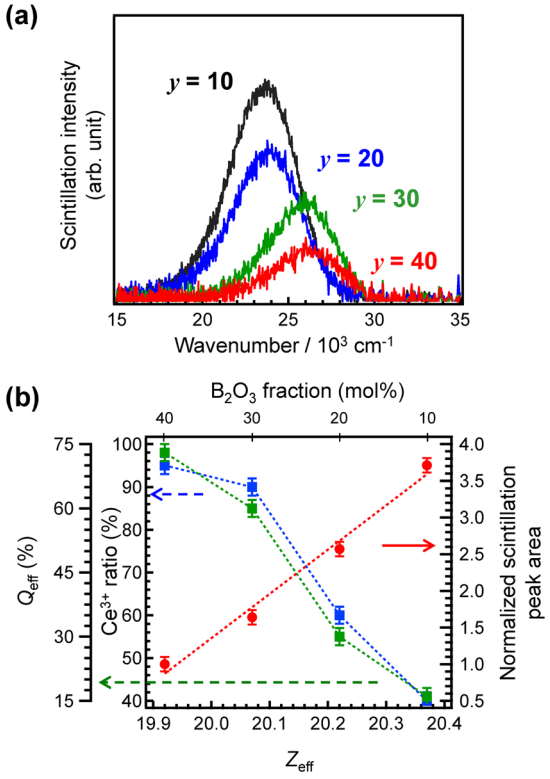

Figure 8. Scintillation properties of 0.5Ce:LBS*y* glasses. (**a**) X-ray-induced scintillation spectra of 0.5Ce:LBS*y* glasses by an irradiation dose of 10 Gy. (**b**) Values of Q_{eff}, the *Ce^{3+} ratio*, and the normalized scintillation peak area as a function of Z_{eff} and the B_2O_3 fraction.

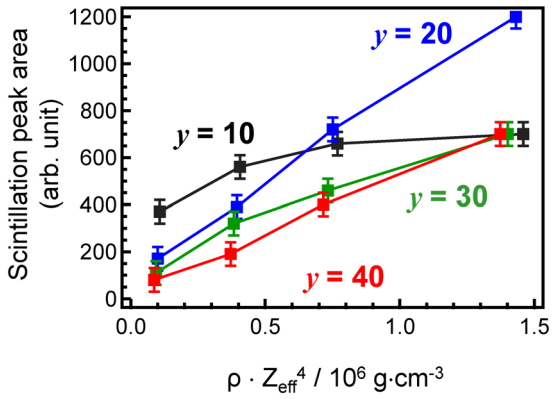

Figure 9. X-ray-induced scintillation peak area of *x*Ce:LBS*y* glasses as a function of $\rho \cdot Z_{eff}^4$ for different B_2O_3 fractions.

mixture of Li_2CO_3 (99.99%), B_2O_3 (99.9%), SiO_2 (99.999%), and $Ce(OCOCH_3)_3 \cdot 2H_2O$ (99.9%) was melted in an electric furnace at 1100°C for 30 min in an Ar atmosphere (99.999%). The glass melt was quenched on a stainless plate at 200°C and then annealed at a temperature T_g, which was measured by differential thermal analysis (DTA) for 1 h. The bulk glasses were cut into several glass pieces (10 mm × 10 mm) using a cutting machine, and then, samples were mechanically polished (thickness ~ 1 mm) to obtain mirror surfaces. The temperature T_g was determined by a DTA system operating at a heating rate of 10 °C/min using a TG8120 instrument (Rigaku, Japan). The density of the samples was measured using the Archimedes method with pure water as an immersion liquid.

Luminescence properties. The PL and PLE spectra were recorded at 1 nm intervals at RT using an F7000 fluorescence spectrophotometer (Hitachi High-Tech. Japan). Band pass filters of 2.5 nm for the PL measurement were used for both excitation and emission. The absorption spectra at RT were recorded at 1 nm intervals using a U3500 UV-vis-NIR spectrometer (Hitachi High-Tech. Japan). The absolute quantum efficiencies, also known as quantum yields (QYs), of the glasses were measured using an integrating sphere Quantaurus-QY (Hamamatsu

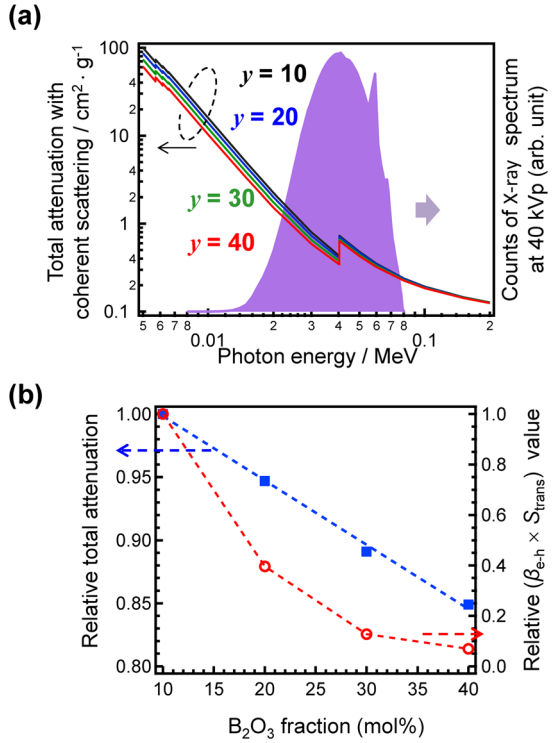

Figure 10. Total attenuation of 0.5Ce:LBS*y* glasses. (**a**) Total attenuation with coherent scattering of 0.5Ce:LBS*y* glasses. The scale of the spectrum of the tungsten lamp is given on the right y-axis. (**b**) Total attenuation and ($\beta_{e\text{-}h} \times S_{trans}$) relative to the values for the 0.5Ce:LBS10 glass.

Photonics, Japan). The error bars were ±2. The emission decay at RT was measured using a Quantaurus-Tau system (Hamamatsu Photonics, Japan) with a 340 nm LED. The accumulated counts for evaluation were 50,000. Scintillation (radioluminescence) spectra were measured by using a CCD-based spectrometer (Andor DU920P CCD and SR163 monochromator) under X-ray exposure[23]. The supplied bias voltage and tube current were 40 kV and 0.52 ~ 5.2 mA, respectively.

XANES measurement. The Ce L_{III}-edge XANES spectra were measured at the BL01B1 and BL14B2 beamlines of SPring-8 (Hyogo, Japan). The storage ring energy was operated at 8 GeV with a typical current of 100 mA. The measurements were performed using a Si (111) double-crystal monochromator in the transmission mode (Quick Scan method), or in the fluorescence mode using 19-SSD detector at RT. The XANES spectra were recorded from 5.52 to 6.18 keV. Pellet samples for the measurements were prepared by mixing the granular sample with boron nitride. As references, XANES data for $Ce(OCOCH_3)_3{\cdot}2H_2O$ and CeO_2 were collected using the same conditions. The corresponding analyses were performed by using Athena software[53].

References

1. Yen, W. M., Shionoya, S. & Yamamoto, H. *Phosphor Handbook 2nd Edition* (CRC Press, 2007).
2. Blasse, G. & Bril, A. Investigation of some Ce^{3+}-activated phosphors. *J. Chem. Phys.* **47**, 5139–5145 (1967).
3. Bachmann, V., Ronda, C. & Meijerink, A. Temperature quenching of yellow Ce^{3+} luminescence in YAG:Ce. *Chem. Mater.* **10**, 2077–2084 (2009).
4. Pollnau, M., Gamelin, D. R., Luthi, S. R., Gudel, H. U. & Hehlen, M. P. Power dependence of upconversion luminescence in lanthanide and transition-metal-ion systems. *Phys. Rev. B* **61**, 3337–3346 (2000).
5. Blasse, G. & Bril, A. Study of energy transfer from Sb^{3+}, Bi^{3+}, Ce^{3+} to Sm^{3+}, Eu^{3+}, Tb^{3+}, Dy^{3+}. *J. Chem. Phys.* **47**, 1920–1926 (1967).
6. Matsuzawa, T., Aoki, Y., Takeuchi, N. & Murayama, Y. New long phosphorescent phosphor with high brightness, $SrAl_2O_4$:Eu^{2+},Dy^{3+}. *J. Electrochem. Soc.* **143**, 2670–2673 (1996).
7. Xie, R. J. & Hirosaki, N. Silicon-based oxynitride and nitride phosphors for white LEDs - A review. *Sci. Technol. Adv. Mater.* **8**, 588–600 (2007).
8. Reisfeld, R. Spectra and energy transfer of rare earths in inorganic glasses. *Structure and Bonding* **13**, 53–98 (1973).
9. Layne, C. B., Lowdermilk, W. H. & Weber, M. J. Multiphonon relaxation of rare-earth ions in oxide glasses. *Phys. Rev. B.* **16**, 10–20 (1977).
10. Shinn, M. D., Sibley, W. A., Drexhage, M. G. & Brown, R. N. Optical-transitions of Er^{3+} ions in fluorozirconate glass. *Phys. Rev. B* **27**, 6635–6648 (1983).
11. Schreiber, H. D. *et al.* Compositional dependence of redox equilibria in sodium-silicate glasses. *J. Non-Cryst. Solids* **177**, 340–346 (1994).
12. Duffy, J. A. & Kyd, G. O. Ultraviolet absorption and fluorescence spectra of cerium and the effect of glass composition. *Phys. Chem. Glass* **37**, 45–48 (1996).
13. Skuja, L. Optically active oxygen-deficiency-related centers in amorphous silicon dioxide. *J. Non-Crystal. Solids* **239**, 16–48 (1998).
14. Ebendorff-Heidepriem, H. & Ehrt, D. Formation and UV absorption of cerium, europium and terbium ions in different valencies in glasses. *Opt. Mater.* **15**, 7–25 (2000).

15. Paulose, P. I., Jose, G., Thomas, V., Unnikrishnan, N. V. & Warrier, M. K. R. Sensitized fluorescence of Ce^{3+}/Mn^{2+} system in phosphate glass. *J. Phys. Chem. Solids* **64**, 841–846 (2003).
16. Caldino, U., Hernandez-Pozos, J. L., Flores, C., Speghini, A. & Bettinelli, M. Photoluminescence of Ce^{3+} and Mn^{2+} in zinc metaphosphate glasses. *J. Phys.: Condens. Matter.* **17**, 7297–7305 (2005).
17. Murata, T., Sato, M., Yoshida, H. & Morinaga, K. Compositional dependence of ultraviolet fluorescence intensity of Ce^{3+} in silicate, borate, and phosphate glasses. *J. Non-Cryst. Solids* **351**, 312–316 (2005).
18. Bei, J. F. *et al.* Optical properties of Ce^{3+}-doped oxide glasses and correlations with optical basicity. *Mater. Res. Bull.* **42**, 1195–1200 (2007).
19. Masai, H., Takahashi, Y., Fujiwara, T., Matsumoto, S. & Yoko, T. High photoluminescent property of low-melting Sn-doped phosphate glass. *Appl. Phys. Express* **3**, 082102 (2010).
20. Masai, H. *et al.* Correlation between preparation conditions and the photoluminescence properties of Sn^{2+} centers in $ZnO\text{-}P_2O_5$ glasses. *J. Mater. Chem. C* **2**, 2137–2143 (2014).
21. Combes, C. M., Dorenbos, P., van Eijk, C. W. E., Krämer, K. W. & Güdel, H. U. Optical and scintillation properties of pure and Ce^{3+}-doped Cs_2LiYCl_6 and Li_3YCl_6: Ce^{3+} crystals. *J. Lumin.* **82**, 299–305 (1999).
22. Dorendos, P. *et al.* 4f-5d spectroscopy of Ce^{3+} in $CaBPO_5$, $LiCaPO_4$ and Li_2CaSiO_4. *J. Phys. Condens. Matter.* **15**, 511–520 (2003).
23. Yanagida, T., Kamada, K., Fujimoto, Y., Yagi, H. & Yanagitani, T. Comparative study of ceramic and single crystal Ce:GAGG scintillator. *Opt. Mater.* **35**, 2480–2485 (2013).
24. Masai, H. & Yanagida, T. Emission property of Ce^{3+}-doped $Li_2O\text{-}B_2O_3\text{-}SiO_2$ glasses. *Opt. Mater. Express* **5**, 1851–1858 (2015).
25. Yanagida, T., Ueda, J., Masai, H., Fujimoto, Y. & Tanabe, S. Optical and scintillation properties of Ce-doped $34Li_2O\text{-}5MgO\text{-}10Al_2O_3\text{-}51SiO_2$ glass. *J. Non-Cryst. Solids* **431**, 140–144 (2016).
26. Torimoto, A. *et al.* Emission properties of Ce^{3+} centers in barium borate glasses prepared from different precursor materials. *Opt. Mater.* **72**, 52–57 (2017).
27. van Eijk, C. W. E., Bessiére, A. & Dorenbos, P. Inorganic thermal-neutron scintillators. *Nucl. Instrum. Meth. A* **529**, 260–267 (2004).
28. Kouzes, R. T. *et al.* Neutron detection alternatives to ^3He for national security applications. *Nucl. Instrum. Meth. A* **623**, 1035–1045 (2010).
29. Iwanowska, J. *et al.* Thermal neutron detection properties with Ce^{3+} doped $LiCaAlF_6$ single crystals. *Nucl. Instrum. Meth. A* **652**, 319–322 (2011).
30. Mizukami, K. *et al.* Measurements of performance of a pixel-type two-dimensional position sensitive Li-glass neutron. *Nucl. Instrum. Meth. A* **529**, 310–312 (2004).
31. Ishii, M. *et al.* Boron based oxide scintillation glass for neutron detection. *Nucl. Instrum. Meth. A* **537**, 282–285 (2005).
32. Masai, H. *et al.* Local coordination state of rare earth in eutectic scintillators for neutron detector applications. *Sci. Rep.* **5**, 13332 (2015).
33. Torimoto, A. *et al.* Emission properties of Ce-doped alkaline earth borate glasses for scintillator applications. *Opt. Mater.* **73**, 517–522 (2017).
34. Yanagida, T. Ionizing radiation induced emission: Scintillation and storage-type luminescence. *J. Lumin.* **169**, 544–548 (2016).
35. Nanto, H. *et al.* Optically stimulated luminescence in x-ray irradiated xSnO–$(25\text{-}x)$SrO–$75B_2O_3$ glass. *Nucl. Instrum. Meth. A* **784**, 14–16 (2015).
36. Atari, N. A. Piezoluminescence phenomenon. *Phys. Lett.* **90A**, 93–96 (1982).
37. Xu, C. N., Watanabe, T., Akiyama, M. & Zheng, X. G. Artificial skin to sense mechanical stress by visible light emission. *Appl. Phys. Lett.* **74**, 1236–1238 (1999).
38. Jackson, D. F. & Hawkes, D. J. X-ray attenuation coefficients of elements and mixtures. *Phys. Reports* **70**, 169–233 (1981).
39. Knoll, G. F. Radiation Detection and Measurement, Fourth Edition, John Wiley & Sons (2012).
40. Robbins, D. J. On predicting the maximum efficiency of phosphor systems excited by ionizing radiation. *J. Electrochem. Soc.* **127**, 2694–2702 (1980).
41. Lempicki, A., Wojtowicz, A. J. & Berman, E. Fundamental limits of scintillator performance. *Nucl. Instrum. Methods Phys. Res. A* **333**, 304–311 (1993).
42. Duffy, J. A. & Ingram, M. D. An interpretation of glass chemistry in terms of the optical basicity concept. *J. Non-Crystal. Solids* **21**, 373–410 (1976).
43. Duffy, J. A. A review of optical basicity and its applications to oxidic systems. *Geochim. Cosmochim. Acta.* **57**, 3961–3970 (1993).
44. Masai, H., Matsumoto, S., Ueda, Y. & Koreeda, A. Correlation between valence state of tin and elastic modulus of Sn-doped $Li_2O\text{–}B_2O_3\text{–}SiO_2$ glasses. *J. Appl. Phys.* **119**, 185104 (2016).
45. http://physics.nist.gov/PhysRefData/Xcom/html/xcom1.html.
46. Boone, J. M., Fewell, T. R. & Jennings, R. J. Molybdenum, rhodium, and tungsten anode spectral models using interpolating polynomials with application to mammography. *Med. Phys.* **24**, 1883–1874 (1997).
47. Boone, J. M. & Seibert, J. A. An accurate method for computer-generating tungsten anode x-ray spectra from 30 to 140 kV. *Med. Phys.* **24**, 1661–1670 (1997).
48. Fewell, T. R., Shuping, R.E. & Healy, K. *Handbook of Computed Tomography X-ray Spectra*; HHS Publication (FDA) 81-8162. (Rockville, MD, 1981).
49. Wu, Y. T., Meng, F., Li, Q., Koschan, M. & Melcher, C. L. Role of Ce^{4+} in the scintillation mechanism of codoped $Gd_3Ga_3Al_2O_{12}$: Ce. *Phys. Rev. Appl.* **2**, 044009 (2014).
50. Zavartsev, Y. D., Koutovoi, S. A. & Zagumennyi, A. I. Czochralski growth and characterisation of large Ce^{3+}:Lu_2SiO_5 single crystals co-doped with Mg^{2+} or Ca^{2+} or Tb^{3+} for scintillators. *J. Crystal Growth.* **275**, e2167–e2171 (2005).
51. Nikl., M. *et al.* The stable Ce^{4+} center: A new tool to optimize Ce-doped oxide scintillators. *IEEE Trans. Nucl. Sci.* **63**, 433–438 (2016).
52. Mansuy, C., Nedelec, J. M. & Mahiou, R. Molecular design of inorganic scintillators: from alkoxides to scintillating materials. *J. Mater. Chem.* **14**, 3274–3280 (2004).
53. Ravel, B. & Newville, M. ATHENA, ARTEMIS, HEPHAESTUS: data analysis for X-ray absorption spectroscopy using IFEFFIT. *J. Synchrotron Radiat.* **12**, 537–541 (2005).

Acknowledgements

This work was partially supported by the JSPS KAKENHI Grant-in-Aid for Young Scientists (A) Number 26709048, and the Collaborative Research Program of I.C.R., Kyoto University (grants #2015-40 and #2016-83). The synchrotron radiation experiments were performed at the BL14B2 of SPring-8 with the approval of the Japan Synchrotron Radiation Research Institute (JASRI) (Proposal Nos. 2015B1587, 2016A0130, 2016B0130, 2017A0130, and 2017B0130).

Author Contributions

H.M. formulated the research project. H.M. and T.U. performed the materials preparation. H.M. and A.T. performed the XANES analysis. H.M., G.O., N.K. and T.Y. measured the X-ray-induced scintillation. H.M. and G.O. wrote the paper. All authors discussed the results.

Additional Information

Supplementary information accompanies this paper at https://doi.org/10.1038/s41598-017-18954-y.

Competing Interests: The authors declare that they have no competing interests.

Publisher's note: Springer Nature remains neutral with regard to jurisdictional claims in published maps and institutional affiliations.